A TMA-FDA Approach for Two-Beam Steering

Roberto Maneiro-Catoira, *Member, IEEE,* Julio Brégains, *Senior Member, IEEE,*
José A. García-Naya, *Senior Member, IEEE,* and Luis Castedo, *Senior Member, IEEE*

***Abstract*—Frequency diverse arrays (FDAs) allow the synthesis of dot-shaped radiated patterns in the range-angle space by applying frequency offsets to the antenna elements. Conventional FDAs are usually implemented with costly variable phase shifters and mixers, and require an independent feeding network per beam for multi-beam operation. In this letter, we propose an innovative approach to FDA that makes use of time-modulated array (TMA) building blocks modeled with inexpensive single-pole dual-throw (SPDT) switches. Our approach is able to simultaneously and independently steer two dot-shaped beam patterns, over the two most significant TMA harmonics, with an almost 90% time modulation efficiency.**

***Index Terms*—Frequency Diverse Arrays, Time-modulated arrays.**

I. Introduction

FREQUENCY Diverse Arrays (FDAs) are attractive due to their ability to synthesize dot-shaped radiated patterns in range-angle space [1]–[3]. FDAs have promising applications in interference mitigation [4] or secure communications [5]. In general, they are implemented with analog feeding networks having variable phase shifters (VPSs) and mixers [6]–[8], devices with high cost and insertion losses, both increasing with the carrier frequency. VPSs also suffer from limited phase resolution [9], [10]. These drawbacks are even greater if a simultaneous multi-target is addressed. As a matter of fact, attempts not to replicate the FDA multi-target feeding networks result in less flexible beam steering approaches whose design is either restricted to targets within the same range r [11] or is set to utilize time-multiplexed windows to focus on each target [12]. These approaches do not allow simultaneous multi-target beam steering.

An alternative is to replace conventional FDA feeding networks with time-modulated array (TMA) switched architectures where periodical (with period T_0) rectangular pulses are applied to the individual excitations of an antenna array by means of radio frequency (RF) switches. Conventional TMAs generate radiation patterns at frequencies $f_c \pm q f_0$, $q \in \mathbb{N}$ (suitable only to angle-dependent multi-focusing applications [13], [14]) being f_c the carrier frequency, λ_c its wavelength, and $f_0 = 1/T_0$ is the time-modulation fundamental frequency.

Manuscript received ————; accepted ————. Date of publication ————; date of current version ————. This work has been funded by the Xunta de Galicia (by grant ED431C 2020/15, and grant ED431G 2019/01 to support the Centro de Investigación de Galicia "CITIC"), the Agencia Estatal de Investigación of Spain (by grants RED2018-102668-T and PID2019-104958RB-C42) and ERDF funds of the EU (FEDER Galicia 2014-2020 & AEI/FEDER Programs, UE). *(Corresponding author: José A. García-Naya.)*

The authors are with the CITIC Research Center, University of A Coruña, Spain. (email: roberto.maneiro@udc.es, julio.bregains@udc.es, jagarcia@udc.es, luis@udc.es)

Digital Object Identifier

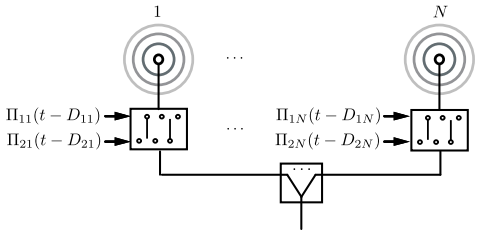

Fig. 1. Proposed FDA-TMA architecture for dual-focusing without VPSs or mixers, but switched feeding networks controlled by the square periodic sequences $\Pi_{kn}(t - D_{kn})$, with $k \in \{1, 2\}$ and $n \in \{1, \ldots, N\}$.

This letter contains two significant contributions: 1) the generation of the FDA frequency offsets by simply varying the frequency of the periodic square pulses that govern a TMA feeding network, hence FDA capabilities[1] are incorporated without using VPSs and RF mixers but RF switches, which allow an easy and accurate control of the frequency offsets by means of the switching on-off instants; 2) the exploitation of the multibeam single-sideband TMAs developed in [20], which exhibits an excellent level of modulation efficiency and beam scanning flexibility, as a building block for multi-target FDAs. In this letter we consider the case of two independently-steerable dot-shaped beams, but similar ideas are applicable to TMA architectures capable of synthesizing more beams [20]. Note that TMAs and FDAs were considered in [21], but limited to a single beam and array elements controlled by identical bipolar squared pulses with a fixed frequency.

II. Signal model

Fig. 1 shows the block diagram of a uniformly excited N-element antenna array with the proposed TMA feeding network which we will design to work as a two-beam FDA. We assume a pulsed input signal $s(t) = \text{rect}(t/T_p)\text{e}^{\text{j}2\pi f_c t}$, with pulse repetition interval T_r, where $\text{rect}(t/T_p)$=1 if $|t| \leq T_p/2$ and 0 otherwise, being T_p the pulse duration ($T_p \ll T_r$). The signals at the output of the antenna elements after time modulation are

$$s_n(t) = h_n(t)s(t), \;\; n = 1, \ldots, N \tag{1}$$

where $h_n(t)$ is the n-th element time-modulated excitation constructed as explained in Fig. 2. The starting point is the four-level stair-step pulse $p_{kn}(t)$, $k \in \{1, 2\}$ and $n \in \{1, \cdots, N\}$ shown in Fig. 2a which results from the sum of the three bipolar square pulses $a_{kn}(t)$, $b_{kn}(t)$, and $c_{kn}(t)$ [20]. The signals $p_{kn}(t)$ are periodic with fundamental period T_{kn}.

[1]Given the circumstance that the single maximum in the dot-shaped patterns are not static in time [15]–[19], this work is limited to the study of instantaneous dot-shaped beampatterns for a given time t_0.

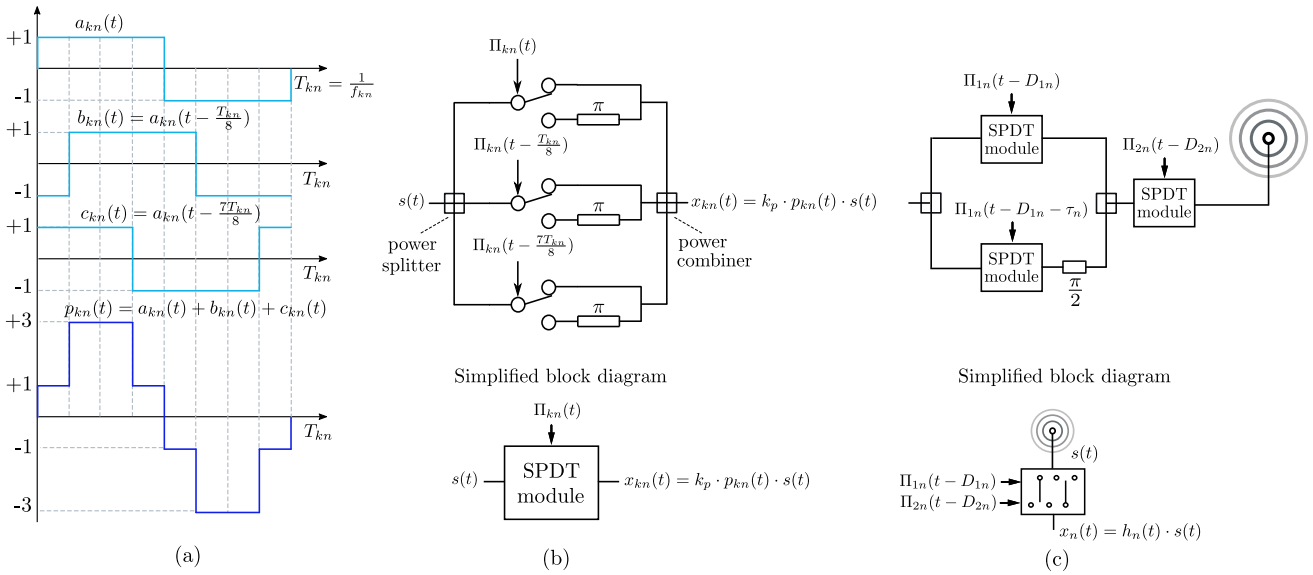

Fig. 2. (a) Construction of a periodic four-level stair-step pulse $p_{kn}(t)$ from bipolar squared sequences. (b) Architecture with SPDT switches to synthesize $p_{kn}(t)$ and the corresponding simplified block. Notice that the squared unipolar control signal $\Pi_{kn}(t)$ takes the values $\Pi_{kn}(t) = 1$ when $a_{kn}(t) \geq 0$ and $\Pi_{kn}(t) = 0$ when $a_{kn}(t) < 0$. (c) Block diagram of the n-th element feeding network of the proposed TMA-FDA approach that allows for steering independently two harmonic dot-shaped beam patterns in the range-angle space.

Time modulating with $p_{kn}(t)$ is efficiently implemented with the SPDT switches connection in Fig. 2b, which is controlled by delayed versions of a unipolar square pulse $\Pi_{kn}(t)$, also periodic with fundamental period T_{kn}. The output signal of the SPDT module in Fig. 2b is $x_{kn}(t) = k_p p_{kn}(t) s(t)$, where $k_p = 1/\sqrt{5}$ is a normalizing constant resulting from matching the powers of $s(t)$ and $x_{kn}(t)$. Note that SPDT switches waste no power since they never reach the off-state [20].

Next, two SPDT modules are connected as in Fig. 2c to construct a single sideband (SSB) TMA module. As explained bellow, a feeding network with such modules steers two dot-shaped beampatterns independently in the range-angle domain, while removing the harmful frequency-mirrored beampatterns produced in conventional TMAs. Indeed, according to Fig. 2c, the signal collected by the n-th antenna element is evenly distributed between two branches by means of a 2-way splitter. The signal in the upper branch inputs a SPDT module controlled by the periodic unipolar signal $\Pi_{1n}(t - D_{1n})$, being $D_{1n} \in [0, T_{1n}]$ a time delay, and is therefore time modulated by the periodic stair-step signal $p_{1n}(t - D_{1n})$ with fundamental frequency $f_{1n} = 1/T_{1n}$. In the lower branch, the signal goes through another SPDT module controlled by $\Pi_{1n}(t - D_{1n} - \tau_n)$, with τ_n being a fixed time delay such that $2\pi f_{1n}\tau_n = \pi/2$ [14], followed by a $\pi/2$ phase shifter. This corresponds to time modulating with the periodic stair-step signal $\mathrm{j}p_{1n}(t - D_{1n} - \tau_n)$.

The signals from the two branches input a 2-way combiner whose output goes through a third SPDT module with control signal $\Pi_{2n}(t - D_{2n})$, being $D_{2n} \in [0, T_{2n}]$ another time delay, and is therefore time modulated by the periodic stair-step signal $p_{2n}(t - D_{2n})$ with fundamental frequency $f_{2n} = 1/T_{2n}$. By properly selecting D_{1n}, D_{2n}, f_{1n}, and f_{2n}, the proposed TMA-FDA feeding network steers two dot-shaped beampatterns towards the coordinates (r_1, θ_1) and (r_2, θ_2), respectively.

According to Fig. 2, the n-th element time-modulated excitation is

$$h_n(t) = \left[\frac{k_p p_{1n}(t - D_{1n})}{\sqrt{2}} + \mathrm{j}\frac{k_p p_{1n}(t - D_{1n} - \tau_n)}{\sqrt{2}}\right] \cdot \cdot k_p p_{2n}(t - D_{2n}) \tag{2}$$

Knowing that $p_{1n}(t)$ and $p_{2n}(t)$ have the same Fourier series coefficients $P_m = \frac{1}{\mathrm{j}\pi m}\left(2 - 2\sqrt{2} \cdot (-1)^{(m+3)(m+5)/8}\right)$, with $m \in \mathbb{Z}$, and that $\mathrm{e}^{-\mathrm{j}2\pi m f_{1n}\tau_n} = (-\mathrm{j})^m$ as a consequence of $2\pi f_{1n}\tau_n = \pi/2$, $h_n(t)$ in (2) can be represented by its Fourier series expansion

$$\begin{aligned} h_n(t) &= \frac{k_p^2}{\sqrt{2}}\left[\sum_{q \text{ odd}} \left(1 - (-\mathrm{j})^{q+1}\right) P_q \mathrm{e}^{-\mathrm{j}2\pi q f_{1n} D_{1n}} \mathrm{e}^{\mathrm{j}2\pi q f_{1n} t}\right] \cdot \\ &\cdot \left[\sum_{i \text{ odd}} P_i \mathrm{e}^{-\mathrm{j}2\pi i f_{2n} D_{2n}} \mathrm{e}^{\mathrm{j}2\pi i f_{2n} t}\right] = \\ &= \sqrt{2} k_p^2 \left[\sum_{q \in \Psi} P_q \mathrm{e}^{-\mathrm{j}2\pi q f_{1n} D_{1n}} \mathrm{e}^{\mathrm{j}2\pi q f_{1n} t}\right] \cdot \\ &\cdot \left[\sum_{i \text{ odd}} P_i \mathrm{e}^{-\mathrm{j}2\pi i f_{2n} D_{2n}} \mathrm{e}^{\mathrm{j}2\pi i f_{2n} t}\right] \end{aligned} \tag{3}$$

where $\Psi = \{q = 4\Gamma - 3; \Gamma \in \mathbb{Z}\} = \{\dots, -7, -3, 1, 5, \dots\}$ is the set of nonzero harmonics in the first sum in (3) [20]. We now introduce the following dynamic excitations as

$${}_i^q I_n = |{}_i^q I_n| \mathrm{e}^{\mathrm{j}\left({}_i^q \Phi_n\right)} = \sqrt{2} k_p^2 P_q P_i \mathrm{e}^{-\mathrm{j}2\pi(q f_{1n} D_{1n} + i f_{2n} D_{2n})} \tag{4}$$

which allows (3) to be rewritten as

$$h_n(t) = \sum_{q \in \Psi} \sum_{i \text{ odd}} {}_i^q I_n \mathrm{e}^{\mathrm{j}2\pi(q f_{1n} + i f_{2n})t} \tag{5}$$

Notice from (4) that the moduli of the dynamic excitations $|{}_i^q I_n|$ are constant for all n, whereas their phases are ${}_i^q \Phi_n =$

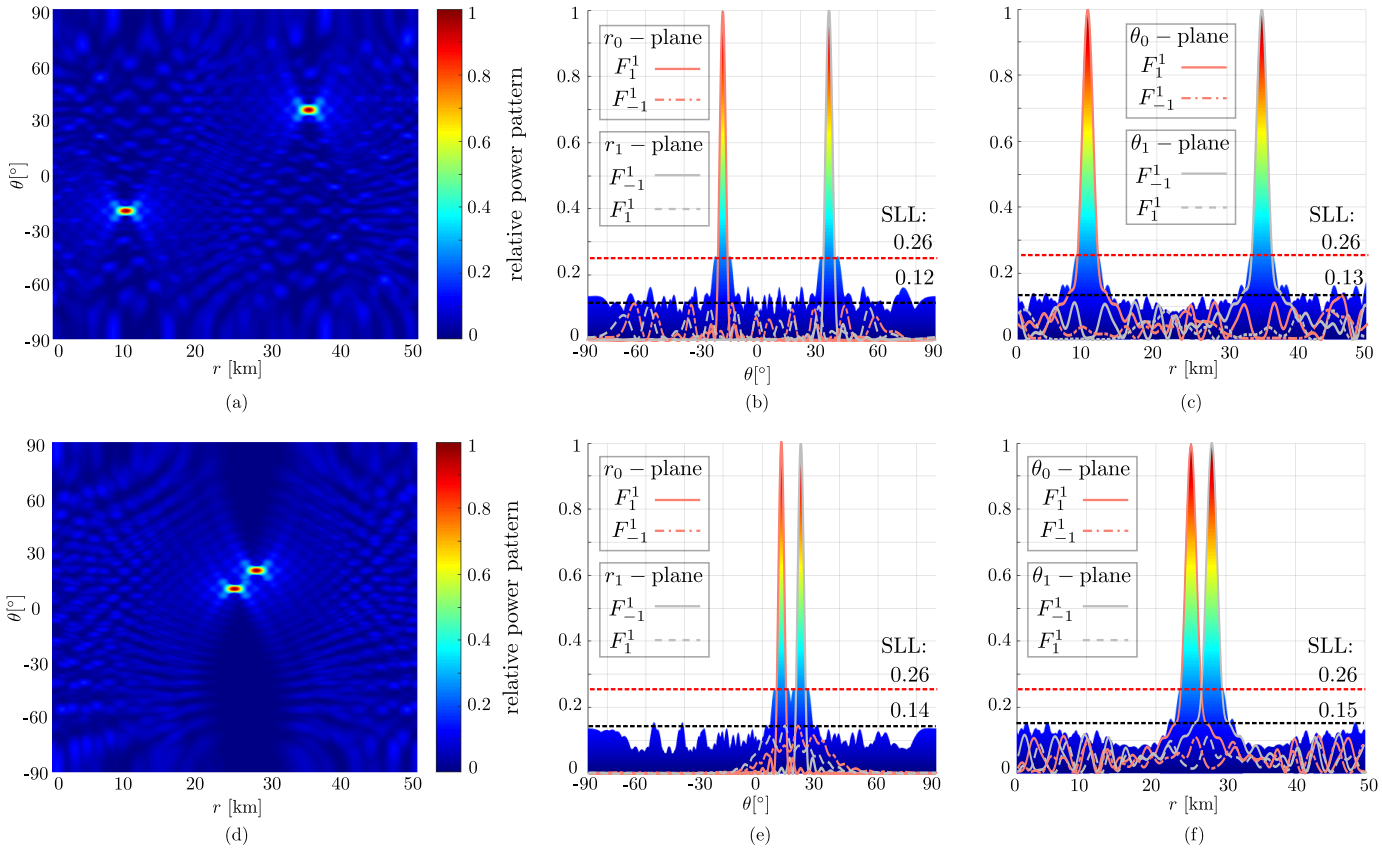

Fig. 3. Projection of the instantaneous spatial focusing beampatterns $|F_1^1(r,\theta)|^2$ and $|F_{-1}^1(r,\theta)|^2$ on the range-angle dimension for N=29 and two different target locations. Additionally, the r_1, r_2, θ_1, and θ_2 plane cuts are shown. The TMA-FDA parameters are α=2.0, f_0=100 MHz, Σf=36.75 kHz, and Δf=35 kHz. Subfigures (a), (b), and (c) in the first row consider (r_1,θ_1)=(10 km, $-20°$) and (r_2,θ_2)=(35 km, $-35°$), and the features of the resulting dot-shaped beam patterns are HPBW$_{r_1}$=2.0 km, HPBW$_{\theta_1}$=3.4°, HPBW$_{r_2}$=1.9 km, and HPBW$_{\theta_2}$=4.2°. The SLL in the corresponding plane cuts is SLL$_{r_1}$=SLL$_{r_2}$=0.12, SLL$_{\theta_1}$=SLL$_{\theta_2}$=0.13, whereas SLL$_\Omega$=0.26 in the whole range-angle sector $\Omega=\{r\in(0\,\text{km},50\,\text{km});\theta\in(-90°,90°)\}$. Subfigures (d), (e), and (f) in the second row consider $(r_1,\theta_1)=(25\,\text{km},10°)$ and $(r_2,\theta_2)=(28\,\text{km},20°)$, and lead to dot-shaped beam patterns with HPBW$_{r_1}$=2.0 km, HPBW$_{\theta_1}$=3.2°, (r_2,θ_2)=(28 km, 20°), HPBW$_{\theta_2}$=3.4°, SLL$_{r_1}$=SLL$_{r_2}$=0.14, SLL$_{\theta_1}$=SLL$_{\theta_2}$=0.15, and SLL$_\Omega$=0.26.

$qf_{1n}D_{1n}+if_{2n}D_{2n}$. Therefore, the radiated power pattern of any harmonic corresponds to that of a uniform linear array and such patterns can be steered by adapting the phase terms ${}_i^q\Phi_n$ by means of the parameters D_{1n}, D_{2n}, f_{1n}, and f_{2n}. Notice also that the most significant harmonics are the ones corresponding to $(q,i)=(1,1)$ and $(q,i)=(1,-1)$, since, according to (4), the following inequality holds: $20\log\left|\frac{{}_1^1I_n}{{}_i^qI_n}\right| = 20\log\left|\frac{{}_{-1}^1I_n}{{}_i^qI_n}\right| \geq 16.9$ dB, $\forall(|q|,|i|)\neq(1,1)$. According to (1) and (5), the signal radiated at an arbitrary probe point of coordinates (r,θ) in space is

$$\begin{aligned}S(t,r,\theta)&=\sum_{n=1}^{N}\frac{1}{r_n}s_n\left(t-\frac{r_n}{c}\right)=\\&=\sum_{n=1}^{N}\frac{\text{rect}(\frac{t}{T_p})}{r_n}\sum_{q\in\Psi}\sum_{i\ \text{odd}}{}_i^qI_n\mathrm{e}^{\mathrm{j}2\pi(qf_{1n}+if_{2n})\left(t-\frac{r_n}{c}\right)}\mathrm{e}^{\mathrm{j}2\pi f_c\left(t-\frac{r_n}{c}\right)}\\&=\sum_{q\in\Psi}\sum_{i\ \text{odd}}\sum_{n=1}^{N}\frac{\text{rect}(\frac{t}{T_p})}{r_n}|{}_i^qI_n|\mathrm{e}^{\mathrm{j}2\pi(f_c+qf_{1n}+if_{2n})\left(t-\frac{r_n}{c}\right)}\mathrm{e}^{\mathrm{j}\left({}_i^q\Phi_n\right)}\end{aligned}\tag{6}$$

where c is the speed of light and $r_n\approx r-(n-1)d\sin\theta$ is the distance between the n-th element and the probe point. We next decompose f_{1n} and f_{2n} as follows

$$f_{1n}=f_0+\frac{\Sigma f_n}{2}+\frac{\Delta f_n}{2},\quad f_{2n}=f_0+\frac{\Sigma f_n}{2}-\frac{\Delta f_n}{2}\tag{7}$$

where f_0 is the fundamental TMA frequency, and Σf_n and Δf_n are two frequency offsets such that $\Sigma f_n>\Delta f_n>0$. If we also assume that $1/r_n\approx 1/r$, we arrive at

$$\begin{aligned}&S(t,r,\theta)=\text{rect}\,(t/T_p)/r\cdot\\&\cdot\sum_{q\in\Psi}\sum_{i\ \text{odd}}\mathrm{e}^{\mathrm{j}2\pi(f_c+(q+i)f_0)\left(t-\frac{r}{c}\right)}\sum_{n=1}^{N}|{}_i^qI_n|\mathrm{e}^{\mathrm{j}\left({}_i^q\Phi_n\right)}\cdot\\&\cdot\mathrm{e}^{\mathrm{j}2\pi\left[\left(\frac{(q+i)\Sigma f_n}{2}+\frac{(q-i)\Delta f_n}{2}\right)\left(t-\frac{r}{c}\right)+\frac{(n-1)(f_c+(q+i)f_0)d\sin\theta}{c}\right]}\cdot\\&\cdot\mathrm{e}^{\mathrm{j}2\pi\left[\frac{(n-1)((q+i)\Sigma f_n+(q-i)\Delta f_n)d\sin\theta}{2c}\right]}\end{aligned}\tag{8}$$

which can be rewritten as

$$S(t,r,\theta)=\frac{\text{rect}(\frac{t}{T_p})}{r}\sum_{q\in\Psi}\sum_{i\ \text{odd}}\mathrm{e}^{\mathrm{j}2\pi(f_c+(q+i)f_0)\left(t-\frac{r}{c}\right)}F_i^q(t,r,\theta)\tag{9}$$

with

$$F_i^q(t,r,\theta)=\sum_{n=1}^{N}{}_i^qI_n|\mathrm{e}^{\mathrm{j}\left({}_i^q\Phi_n\right)}\cdot \\ \cdot\,\mathrm{e}^{\mathrm{j}2\pi\left[\left(\frac{(q+i)\Sigma f_n}{2}+\frac{(q-i)\Delta f_n}{2}\right)\left(t-\frac{r}{c}\right)+\frac{(n-1)(f_c+(q+i)f_0)d\sin\theta}{c}\right]}\cdot \\ \cdot\,\mathrm{e}^{\mathrm{j}2\pi\left[\frac{(n-1)((q+i)\Sigma f_n+(q-i)\Delta f_n)d\sin\theta}{2c}\right]} \quad (10)$$

being the array factor corresponding to the harmonic (q,i).

III. TMA-FDA two-beam steering

Limiting the sum in (9) to the two most significant harmonics $(q,i)=(1,1)$ and $(q,i)=(1,-1)$, the signal radiated at the probe point (r,θ) given by (9) can be approximated as

$$S(t,r,\theta)\approx\frac{\mathrm{rect}(\frac{t}{T_p})}{r}\mathrm{e}^{\mathrm{j}2\pi(f_c+2f_0)\left(t-\frac{r}{c}\right)}F_1^1(t,r,\theta)+ \\ +\frac{\mathrm{rect}(\frac{t}{T_p})}{r}\mathrm{e}^{\mathrm{j}2\pi f_c\left(t-\frac{r}{c}\right)}F_{-1}^1(t,r,\theta) \quad (11)$$

Assuming $|\Sigma f_n+\Delta f_n|<f_0\ll f_c$, the terms $(n-1)(\Sigma f_n+\Delta f_n)d\sin\theta/c$ and $(n-1)(\Sigma f_n-\Delta f_n)d\sin\theta/c$ in $F_1^1(t,r,\theta)$ and $F_{-1}^1(t,r,\theta)$ (see (10)), respectively, can be neglected [6], [11], thus leading to

$$F_1^1(t,r,\theta)\approx\sum_{n=1}^{N}{}_1^1I_n|\mathrm{e}^{\mathrm{j}\left({}_1^1\Phi_n\right)}\mathrm{e}^{\mathrm{j}2\pi\left[\Sigma f_n\left(t-\frac{r}{c}\right)+\frac{(n-1)(f_c+2f_0)d\sin\theta}{c}\right]} \\ F_{-1}^1(t,r,\theta)\approx\sum_{n=1}^{N}{}_{-1}^1I_n|\mathrm{e}^{\mathrm{j}\left({}_{-1}^1\Phi_n\right)}\mathrm{e}^{\mathrm{j}2\pi\left[\Delta f_n\left(t-\frac{r}{c}\right)+\frac{(n-1)f_c+d\sin\theta}{c}\right]} \quad (12)$$

We next consider $\Sigma f_n=\Sigma f\cdot\Upsilon_n$ and $\Delta f_n=\Delta f\cdot\Upsilon_n$, where Σf and Δf are the fixed frequency offsets defined above and

$$\Upsilon_n=\frac{1}{\beta_0(\alpha)}\beta_0\left(\alpha\sqrt{1-\left(\frac{2(n-(N-1)/2)}{N-1}\right)^2}\right) \quad (13)$$

are the weights of a Kaiser window [22, Chapter 5] with α a configuration parameter to adjust the tradeoff between SLL and half power beamwidth (HPBW), and $\beta_0(\cdot)$ the modified Bessel function of the first kind and zero order. We will assume that N is odd for the Kaiser window to be symmetric.

Finally, adjusting the phases of the dynamic excitations as

$$\begin{aligned}{}_1^1\Phi_n&=\frac{2\pi}{c}\left[\Sigma f_n r_1-(n-1)d(f_c+2f_0)\sin\theta_1\right]\\ {}_{-1}^1\Phi_n&=\frac{2\pi}{c}\left[\Delta f_n r_2-(n-1)df_c\sin\theta_2\right]\end{aligned} \quad (14)$$

leads to

$$F_1^1(t,r,\theta)= \\ =\sum_{n=1}^{N}{}_1^1I_n|\mathrm{e}^{\mathrm{j}2\pi\left[\Sigma f_n\left(t-\frac{r-r_1}{c}\right)+\frac{(n-1)(f_c+2f_0)d(\sin\theta-\sin\theta_1)}{c}\right]} \\ F_{-1}^1(t,r,\theta)= \\ =\sum_{n=1}^{N}{}_{-1}^1I_n|\mathrm{e}^{\mathrm{j}2\pi\left[\Delta f_n\left(t-\frac{r-r_2}{c}\right)+\frac{(n-1)f_cd(\sin\theta-\sin\theta_2)}{c}\right]} \quad (15)$$

and it is hence possible to steer these two dot-shaped beams towards the target points (r_1,θ_1) and (r_2,θ_2), respectively.

From (4), the phases of the dynamic excitations of the two most significant harmonics $(q,i)=(1,1)$ and $(q,i)=(1,-1)$ are

$$\begin{aligned}-2\pi(f_{1n}D_{1n}+f_{2n}D_{2n})&={}_1^1\Phi_n\\ -2\pi(f_{1n}D_{1n}-f_{2n}D_{2n})&={}_{-1}^1\Phi_n,\end{aligned} \quad (16)$$

which is a system of linear equations that leads to

$$D_{1n}=-\frac{{}_1^1\Phi_n+\left({}_{-1}^1\Phi_n\right)}{4\pi f_{1n}},\ D_{2n}=-\frac{{}_1^1\Phi_n-\left({}_{-1}^1\Phi_n\right)}{4\pi f_{2n}}. \quad (17)$$

Additionally, recall the time-dependent phases in (15)

$$\begin{aligned}{}_1^1\Theta_n(t)&=2\pi[\Sigma f_n(t-(r-r_1)/c)+\\ &\quad+(n-1)(f_c+2f_0)d(\sin\theta-\sin\theta_1)/c]\\ {}_{-1}^1\Theta_n(t)&=2\pi[\Delta f_n(t-(r-r_2)/c)+\\ &\quad+(n-1)nf_cd(\sin\theta-\sin\theta_2)/c]\end{aligned} \quad (18)$$

whose maximum variation for $t\in(-T_p/2,T_p/2)$ takes place for $(\Sigma f_n)_{\max}$ and is given by $2\pi(N-1)(\Sigma f_n)_{\max}T_p$ [23] and additionally, since, $1/T_p<f_0$ [24], the restriction

$$(N-1)(\Sigma f_n)_{\max}\ll 1/T_p<f_0 \quad (19)$$

ensures $F_1^1(r,\theta)\approx F_1^1(t{=}0,r,\theta)$ and $F_{-1}^1(r,\theta)\approx F_{-1}^1(t{=}0,r,\theta)$ hold. Denoting the whole area $\Omega=\{r\in(r_{\min},r_{\max});\theta\in(-90^\circ,90^\circ)\}$, the time-modulation radiation efficiency of the switched TMA-FDA when $d=\lambda/2$ is given by [14]

$$\eta_{TM}=\frac{\iint_{(r,\theta)\in\Omega}\left[|F_1^1(r,\theta)|^2+|F_{-1}^1(r,\theta)|^2\right]\sin\theta\,d\theta\,dr}{\sum_{q\in\Psi}\sum_{i\ \text{odd}}\iint_{(r,\theta)\in\Omega}|F_i^q(r,\theta)|^2\sin\theta\,d\theta\,dr} \\ =\frac{\sum_{n=0}^{N-1}|{}_1^1I_n|^2+\sum_{n=0}^{N-1}|{}_{-1}^1I_n|^2}{N}=\frac{4k_p^4|P_1|^4N}{N} \\ =\frac{4}{25}\cdot\left(\frac{2+2\sqrt{2}}{\pi}\right)^2=0.893 \quad (20)$$

IV. Numerical results

Fig. 3 plots the resulting two instantaneous dot-shaped beam patterns obtained with the proposed TMA-FDA approach for two different target positions, illustrating its spatial focusing capabilities. We considered T_p=50 ns, T_r=$r_{\max}/c$, f_c=5 GHz, f_0=100 MHz, Σf=36.75 kHz, and Δf=35 kHz (attainable with nanoseconds switches [10], [25]), and α=2.0. The caption of Fig. 3 provides the resulting values for the SLL (below 0.15 in the corresponding r and θ plane cuts, and 0.26 in the whole range-angle sector) as well as HPBW$_r$ and HPBW$_\theta$ in each scenario.

V. Conclusions

We have presented a TMA-FDA approach for the simultaneous and independent steering of two dot-shaped beam patterns. Our approach uses SPDT switches instead of the largely inefficient VPSs and mixers, whereas exhibiting high modulation efficiencies.

REFERENCES

[1] W. Wang, H. C. So, and H. Shao, "Nonuniform frequency diverse array for range-angle imaging of targets," *IEEE Sensors Journal*, vol. 14, no. 8, pp. 2469–2476, 2014.

[2] W. Khan, I. M. Qureshi, and S. Saeed, "Frequency diverse array radar with logarithmically increasing frequency offset," *IEEE Antennas and Wireless Propagation Letters*, vol. 14, pp. 499–502, 2015.

[3] H. Shao, J. Dai, J. Xiong, H. Chen, and W. Wang, "Dot-shaped range-angle beampattern synthesis for frequency diverse array," *IEEE Antennas and Wireless Propagation Letters*, vol. 15, pp. 1703–1706, 2016.

[4] J. Xiong, W. Wang, H. Shao, and H. Chen, "Frequency diverse array transmit beampattern optimization with genetic algorithm," *IEEE Antennas and Wireless Propagation Letters*, vol. 16, pp. 469–472, 2017.

[5] A. Basit, I. M. Qureshi, W. Khan, S. u. Rehman, and M. M. Khan, "Beam pattern synthesis for an fda radar with hamming window-based nonuniform frequency offset," *IEEE Antennas and Wireless Propagation Letters*, vol. 16, pp. 2283–2286, 2017.

[6] A. Yao, W. Wu, and D. Fang, "Frequency diverse array antenna using time-modulated optimized frequency offset to obtain time-invariant spatial fine focusing beampattern," *IEEE Transactions on Antennas and Propagation*, vol. 64, no. 10, pp. 4434–4446, 2016.

[7] A. Yao, P. Rocca, W. Wu, and A. Massa, "On the design of frequency diverse arrays for wireless power transmission," in *2017 11th European Conference on Antennas and Propagation (EUCAP)*, 2017, pp. 900–903.

[8] S. Y. Nusenu and A. Basit, "Frequency diverse array antennas: From their origin to their application in wireless communication systems," *Journal of Computer Networks and Communications*, vol. 2018, 2018.

[9] "Qorvo," http://www.qorvo.com, monolithic microwave integrated circuit (MMIC) digital phase shifters. Accessed: 2021-02-02.

[10] "Analog devices," https://www.analog.com, SPDT switches. HMC284AMS8G, HMC545A. HMC649A, HMC642A. Accessed: 2021-01-02.

[11] A. Yao, W. Wu, and D. Fang, "Solutions of time-invariant spatial focusing for multi-targets using time modulated frequency diverse antenna arrays," *IEEE Transactions on Antennas and Propagation*, vol. 65, no. 2, pp. 552–566, 2017.

[12] A. Yao, P. Rocca, W. Wu, A. Massa, and D. Fang, "Synthesis of time-modulated frequency diverse arrays for short-range multi-focusing," *IEEE Journal of Selected Topics in Signal Processing*, vol. 11, no. 2, pp. 282–294, 2017.

[13] P. Rocca, Q. Zhu, E. Bekele, S. Yang, and A. Massa, "4-D arrays as enabling technology for cognitive radio systems," *IEEE Trans. Antennas Propag.*, vol. 62, no. 3, pp. 1102–1116, Mar. 2014.

[14] R. Maneiro Catoira, J. Brégains, J. A. Garcia-Naya, L. Castedo, P. Rocca, and L. Poli, "Performance analysis of time-modulated arrays for the angle diversity reception of digital linear modulated signals," *IEEE J. Sel. Topics Signal Process.*, vol. 11, no. 2, pp. 247–258, Mar. 2017.

[15] M. Fartookzadeh, "Comments on "frequency diverse array antenna using time-modulated optimized frequency offset to obtain time-invariant spatial fine focusing beampattern"," *IEEE Transactions on Antennas and Propagation*, vol. 68, no. 2, pp. 1211–1212, 2020.

[16] W. Wu and D. Fang, "Reply to comments on "frequency diverse array antenna using time-modulated optimized frequency offset to obtain time-invariant spatial fine focusing beampattern"," *IEEE Transactions on Antennas and Propagation*, vol. 68, no. 2, pp. 1213–1213, 2020.

[17] Y. Ding and A. Narbudowicz, "Can frequency diverse array prevent wireless eavesdropping in range domain?" 2019.

[18] K. Chen, S. Yang, Y. Chen, and S.-W. Qu, "Accurate models of time-invariant beampatterns for frequency diverse arrays," *IEEE Transactions on Antennas and Propagation*, vol. 67, no. 5, pp. 3022–3029, 2019.

[19] M. Fartookzadeh, "Frequency diverse arrays (fdas) vs. phased arrays: On the application of fdas for secure wireless communications," 2020.

[20] R. Maneiro-Catoira, J. A. García-Naya, J. C. Brégains, and L. Castedo, "Multibeam single-sideband time-modulated arrays," *IEEE Access*, vol. 8, pp. 151 976–151 989, 2020.

[21] R. Maneiro-Catoira, J. Brégains, J. A. García-Naya, and L. Castedo, "Combining switched TMAs and FDAs to synthesize dot-shaped beampatterns," *submitted to IEEE Antennas and Wireless Propagation Letters*, pp. 1–5, 2021.

[22] K. Prabhu, *Window Functions and Their Applications in Signal Processing (1st ed.)*. CRC Press, 2014.

[23] Y. Xu, X. Shi, J. Xu, and P. Li, "Range-angle-dependent beamforming of pulsed frequency diverse array," *IEEE Transactions on Antennas and Propagation*, vol. 63, no. 7, pp. 3262–3267, 2015.

[24] R. Maneiro-Catoira, J. Brégains, J. A. García-Naya, and L. Castedo, "Time modulated arrays: From their origin to their utilization in wireless communication systems," *Sensors*, vol. 17, no. 3, pp. 1–14, Mar. 2017.

[25] "Macom," https://www.macom.com, sPMT switches: MASW-00x100 Series Accessed: 2021-01-02.